Journal of Veterinary Cardiology (2024) **52**, 1—13

ELSEVIER

Journal of Veterinary Cardiology
ESVC

www.elsevier.com/locate/jvc

Structural and electro-anatomical characterization of the equine pulmonary veins: implications for atrial fibrillation☆

S.T. Kjeldsen [a,*], S.D. Nissen [a], A. Saljic [b], E.M. Hesselkilde [b], H. Carstensen [a], S.M. Sattler [c], T. Jespersen [b], D. Linz [b,d], C. Hopster-Iversen [a], R. Kutieleh [e], P. Sanders [f], R. Buhl [a]

[a] *Department of Veterinary Clinical Sciences, Faculty of Health and Medical Sciences, University of Copenhagen, Agrovej 8, 2630 Taastrup, Denmark*
[b] *Laboratory of Cardiac Physiology, Department of Biomedical Sciences, Faculty of Health and Medical Sciences, University of Copenhagen, Blegdamsvej 3B, 2200 Copenhagen, Denmark*
[c] *Department of Cardiology, Herlev and Gentofte University Hospital, Gentofte Hospitalsvej 1, 2900 Hellerup, Denmark*
[d] *Department of Cardiology, Maastricht University Medical Centre and Cardiovascular Research Institute Maastricht, Universiteitssingel 50, 632, 6229 ER Maastricht, Netherlands*
[e] *Abbott Medical, 214 Greenhill Road, SA 5063, Australia*
[f] *Centre for Heart Rhythm Disorders, Royal Adelaide Hospital and University of Adelaide, Port Rd, SA 5000, Australia*

Received 21 July 2023; received in revised form 3 January 2024; accepted 3 January 2024

☆ A unique aspect of the Journal of Veterinary Cardiology is the emphasis of additional web-based materials permitting the detailing of procedures and diagnostics. These materials can be viewed (by those readers with subscription access) by going to http://www.sciencedirect.com/science/journal/17602734. The issue to be viewed is clicked and the available PDF and image downloading is available via the Summary Plus link. The supplementary material for a given article appears at the end of the page. To view the material is to go to http://www.doi.org and enter the doi number unique to this paper which is indicated at the end of the manuscript.

* Corresponding author.
E-mail address: sofie.troest@sund.ku.dk (S.T. Kjeldsen).

https://doi.org/10.1016/j.jvc.2024.01.001

KEYWORDS
Paroxysmal atrial fibrillation;
Horse;
Animal model;
Electro-anatomical mapping;
Immunohistochemistry

Abstract *Introduction/objectives:* Spontaneous pulmonary vein (PV) activity triggers atrial fibrillation (AF) in humans. Although AF frequently occurs in horses, the origin remains unknown. This study investigated the structural and electro-anatomical properties of equine PVs to determine the potential presence of an arrhythmogenic substrate.
Animals, materials and methods: Endocardial three-dimensional electro-anatomical mapping (EnSite Precision) using high-density (HD) catheters was performed in 13 sedated horses in sinus rhythm. Left atrium (LA) access was obtained retrogradely through the carotid artery. Post-mortem, tissue was harvested from the LA, right atrium (RA), and PVs for histological characterization and quantification of ion channel expression using immunohistochemical analysis.
Results: Geometry, activation maps, and voltage maps of the PVs were created and a median of four ostia were identified. Areas of reduced conduction were found at the veno-atrial junction. The mean myocardial sleeve length varied from 28 $\pm$ 13 to 49 $\pm$ 22 mm. The PV voltage was 1.2 $\pm$ 1.4 mV and lower than the LA (3.4 $\pm$ 0.9 mV, $P < 0.001$). The fibrosis percentage was higher in PV myocardium (26.1 $\pm$ 6.6 %) than LA (14.5 $\pm$ 5.0 %, $P = 0.003$). L-type calcium channel ($Ca_V1.2$) expression was higher in PVs than LA ($P = 0.001$). T-type calcium channels ($Ca_V3.3$), connexin-43, ryanodine receptor-2, and small conductance calcium-activated potassium channel-3 was expressed in PVs.
Conclusions: The veno-atrial junction had lower voltages, increased structural heterogeneity and areas of slower conduction. Myocardial sleeves had variable lengths, and a different ion channel expression compared to the atria. Heterogeneous properties of the PVs interacting with the adjacent LA likely provide the milieu for re-entry and AF initiation.

Abbreviations

3D	three-dimensional
AF	atrial fibrillation
$Ca_V1.2$	L-type calcium channel
$Ca_V3.3$	T-type calcium channel
HCN4	hyperpolarisation-activated cyclic nucleotide-gated potassium channel
HD	high-density
LA	left atrium
LIPV	left inferior pulmonary vein
PV	pulmonary vein
RA	right atrium
RIPV	right inferior pulmonary vein
RSPV	right superior pulmonary vein
RyR2	ryanodine receptor 2

Introduction

Atrial fibrillation (AF) is the most clinically relevant arrhythmia in horses, severely affecting performance and can lead to a grave prognosis for riding horses [1—3]. Atrial fibrillation can occur in otherwise healthy horses as the atrial myocardium may present characteristics favouring arrhythmias, although the early disease mechanisms are not fully understood [4,5].

It is well characterized that AF in humans is predominantly triggered by ectopic activity originating from the myocardial sleeves protruding from the left atrium (LA) into the pulmonary veins (PV) [6—8]. The ectopy can be induced by increased or abnormal automaticity, or micro re-entry circuits [9—11]. Indeed, there is growing evidence that structural heterogeneity in the veno-atrial junction creates a milieu for micro re-entry which plays a role in the maintenance of AF [12—14].

Similarly in horses, a recent case report showed spontaneous PV ectopy resulting in non-sustained AF during three-dimensional (3D) endocardial electro-anatomical mapping, supporting the arrhythmogenic potential of the PVs in horses [15]. The equine PVs drain oxygenated blood from four regions of the two lung lobes into four main ostia,

from which myocardial sleeves of varying length extend from the veno-atrial junction into the PVs [16,17]. The extracellular matrix in the PVs contains collagen, telocytes and fibroblasts, and the veins are surrounded by adipose tissue and neurons with ganglia located close to the veno-atrial junction [16,18].

In humans with AF, the ectopic activity from the PVs can be caused by altered function of calcium handling ion channels, e.g., ryanodine receptor-2 (RyR2) or calcium channels [10]. Several studies have investigated the PV ion channel expression in dogs and rats as animal models of AF [19–21]. In horses, few studies have investigated the atrial potassium-channel expression, but none have investigated the ion channel expression in the PV myocardium [22–24].

The aim of the current study was to investigate if the PVs in horses display structural and electro-anatomical properties that have the potential to initiate or perpetuate AF. We performed an *in vivo* study using: (1) 3D endocardial electro-anatomical mapping to characterize the electrical conductivity in the equine PVs and (2) histological and immunohistochemical analyses to describe the ion channel composition of the PVs compared to the myocardium in LA and right atrium (RA).

Animals, materials and methods

Animals

The study included 13 clinically healthy Standardbred horses; six mares and seven geldings (age 7.2 ± 2.4 years, weight 485 ± 56 kg and height 156 ± 5 cm). Information on each horse can be found in the supplemental Table A (available online). None of the horses had a history of cardiac disease. All horses passed echocardiographic, electrocardiographic, and biochemical examination with trivial findings only. Horses were purchased for the study with written consent from the previous owners and with approval from the local ethics committee and the Danish Animal Experiments Inspectorate (license number: 2016-15-02-01-01128).

Three-dimensional electro-anatomical mapping

The horses were placed in stocks and sedated with a constant rate infusion of 180–360 mL/h of 1.0 mg/mL xylazine, conscious and in a standing state. Three-dimensional electro-anatomical mapping was performed on all horses as previously described [14,24] using a 16-electrode high-density (HD) grid sensor enabled mapping catheter[g] in combination with EnSite Precision.[h] Surface electrodes and system reference patches were placed orthogonally around the heart, and a decapolar diagnostic catheter[i] was placed through the jugular vein into the inferior vena cava as a stable anatomical intracardiac reference. Access to the arterial circulation was created by exposing the carotid artery and placement of an Agilis sheath.[j] Using transthoracic echocardiographic[k] guidance, the HD-grid catheter was retrogradely advanced through the aortic valve into the left ventricle. After the HD-grid was used to access the left ventricle, the Agilis sheath was advanced over the HD-grid catheter and the assembly then directed through the mitral valve using the active curvature of the Agilis sheath. This then allowed free access to the LA allowing full functionality of the HD-grid catheter for mapping. Three-dimensional reconstructions of the LA and PVs were created while simultaneously creating local activation times and peak-to-peak voltage maps during sinus rhythm using the peak of the P-wave on the electrocardiogram as a timing reference. Software criteria were set using the following parameters: Morphology match = 70% to intrinsic sinus P-wave; cycle length tolerance = OFF; speed limit (speed of catheter movement) = OFF; distance threshold = 0.1 mm; signal-to-noise ratio = 3. Signals with a voltage below 0.05 mV, which is the noise level of the system, was classified as electrically silent and voltages between 0.05 and 0.5 mV were considered low voltages [25]. With the horses in normal sinus rhythm, conduction velocity was calculated from the activation maps using the time of activation and distance measured between two electrograms.[l] Analyses were performed offline using appropriate software.[h,l] This study focusses on the data from the PVs and for comparative purposes, we translated the previous enumeration of the PVs (I-IV) by Vandecasteele et al. [16] to the nomenclature used in human literature: (I) = Left inferior PV (LIPV), (II) = right inferior PV (RIPV),

[g] Advisor™ high-density-grid sensor enabled mapping catheter, Abbott Medical, Minnesota, USA.
[h] EnSite Precision™, Abbott Medical, Minnesota, USA.
[i] Livewire™, Abbott Medical, Minnesota, USA.
[j] Agilis sheath Abbot Medical, Minnesota, USA.
[k] Vivid™ iq, GE Healthcare, Broendby, Denmark.
[l] EPLab Research Works© 2021, Pawel Kuklik, https://github.com/ValveDigitalHealth/EPlabResearchWorksApp/.

(III) = right superior PV (RSPV), (IV) = left superior PV.

Tissue collection and fixation

After the procedure, the horse was euthanized with an intravenous injection of pentobarbital[m] (140 mg/kg). The heart was removed instantly and kept in a cold cardioplegic solution while biopsies from the LA free wall, RA free wall and LIPV, including the veno-atrial junction, were collected (Fig. 1). Immediately after dissection, tissue samples for histology and immunohistochemistry were fixated in 10% neutral buffered formalin for 24 h and subsequently stored in 70% ethanol at room temperature and subsequently fixated in paraffin. The formalin-fixed paraffin-embedded tissue was sectioned into 2-μm increments and transferred onto glass slides.

Histology

Sections from all horses at three different sites (LA, RA, and PV) were deparaffinized by a descending series of ethanol (99.9—70%), followed by a xylene substitution[n] and rehydration in water before they were incubated overnight in Bouin's solution.[o] Slides were stained with Picro-sirius red[p] according to the manufacturer's protocol for the connective tissue stain kit. Finally, the glass slides were mounted with Pertex[q] and coverslips. The sections were scanned with 20x objective.[r] ZEN Blue 3.5[s] was used to create subsets (three subsets of 5000 × 5000 pixels and three of 1000 × 1000 pixels) from the images, which were analyzed using automated segmental analysis[t] to distinguish cardiomyocytes, collagen, and background. After separating the different categories, the software provided an overall quantification of the percentage of collagen in the entire area.

[m] Euthasol® vet. (400 mg/mL), Dechra Veterinary Products A/S, Uldum, Denmark.
[n] Tissue-tek® (1466), Sakura, Alphen aan den Rijn, Netherlands.
[o] Bouin's solution (HT10132), Sigma—Aldrich, Merck KGaA, Darmstadt, Germany.
[p] Picro-Sirius Red, Abcam, Cambridge, UK.
[q] Pertex®, Histolab Products AB, Askim, Sweden.
[r] Zeiss Axioscan slide scanner Z1, Carl Zeiss Meditec, Jena, Germany.
[s] ZEN 3.5 Blue edition, Zeiss, Oberkochen, Germany.
[t] ZEN Intellesis trainable segmentation program, Zeiss, Oberkochen, Germany.

Immunohistochemistry

Prior to immunolabelling, sections were deparaffinized as described in the previous paragraph and boiled in citric acid (10 mM). Sections were permeabilized with 0.1 % Triton X-100[u] and washed with phosphate buffered saline before blocking with Bovine Serum Albumin 1% for 1 h at room temperature. Primary antibodies targeting the L-type calcium channel ($Ca_V1.2$), T-type calcium channels ($Ca_V3.3$), connexin-43, RyR2, small conductance calcium-activated potassium channel 3, and hyperpolarization activated cyclic nucleotide-gated potassium channel (HCN4) were diluted in 1% bovine serum albumin and incubated overnight at 4 °C degrees followed by washing. A secondary fluorescence-conjugated antibody was applied and incubated for 1 h. Information on all antibodies and concentrations are listed in supplemental Table B (available online).

After a final triple wash, slides were mounted with Prolong Gold[v] and coverslips. One slide per batch was processed without a primary antibody as a negative control. Images were acquired at 20× objective, using fluorescence microscopy with appropriate filters.[r] Zen Blue 3.5[s] was used to create subsets (10 subsets of 1000 × 1000 pixels per area) from the images, which were analyzed to quantify the fluorescent expression of each protein defined as the number of grey tones. For both the histology and the immunohistochemistry analysis, two sections were missing due to errors in the processing of the fixation (horse #7 PV and horse #13 RA).

Statistical analysis

All statistical analyses were performed in GraphPad Prism.[w] Shapiro—Wilk test and evaluation of Q—Q plots was used to assess for normality. Parametric data are presented as mean and standard deviation and non-parametric data as median and interquartile ranges. A one-way ANOVA was used for multiple comparison without missing values and a mixed-effects analysis was used for multiple comparison with missing values. An unpaired t-test was used to compare the inferior and superior veins and to compare atrial and venous segments. The level of significance was set at P-value <0.05.

[u] Triton-X-100, Sigma—Aldrich, Merck Life Science A/S, Soeborg, Denmark.
[v] Prolong Gold, Invitrogen, ThermoFisher Scientific, Denmark.
[w] GraphPad Prism Software, San Diego, CA, USA.

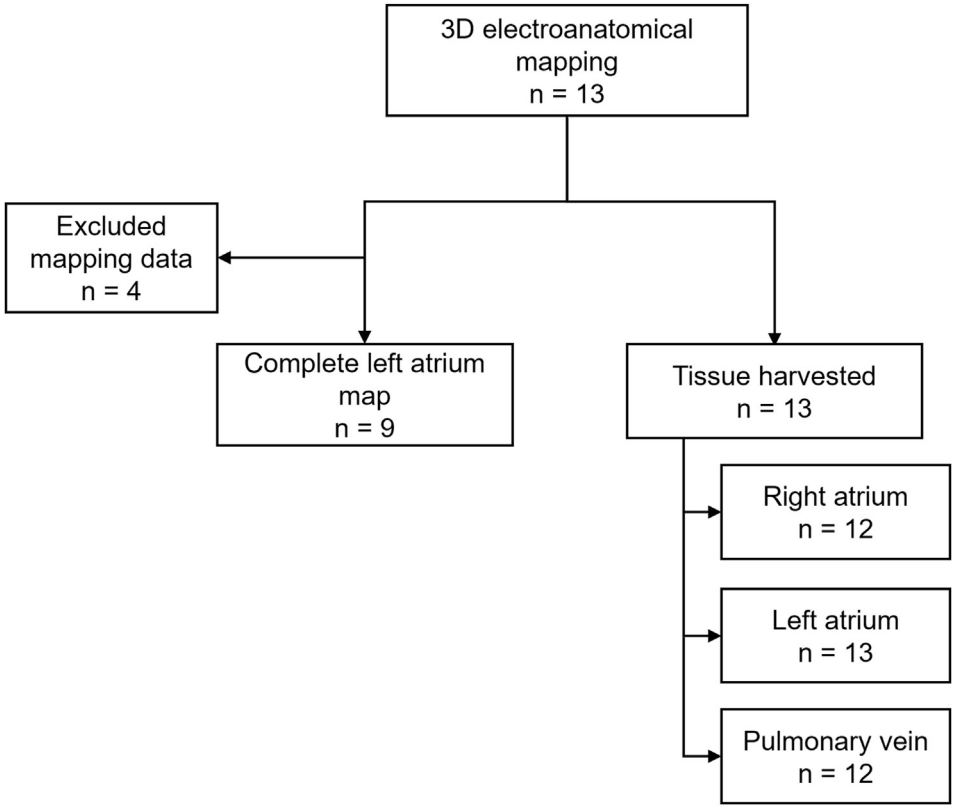

Figure 1 Study overview. Horses and applied method. Thirteen horses underwent three-dimensional (3D) electroanatomical mapping. Mapping data from four horses were excluded because of incomplete datasets resulting in nine complete left atrium maps. Tissue was harvested from all 13 horses from three different sites. Two samples were excluded because of error in the fixation process.

Results

Three dimensional electro-anatomical mapping

We were able to advance the HD-grid into all four pulmonary ostia in seven horses, and three ostia in two horses (#12,13) with a mean number of used points being LIPV 89 $\pm$ 56, RIPV 139 $\pm$ 65, RSPV 217 $\pm$ 93, and left superior PV 99 $\pm$ 104 (Table 1). Branching of the RSPV was observed in five horses, with three being the maximum number of veins. The data collection was successful in nine horses, and four horses were excluded from the analyses, either because of technical errors related to data collection (#3,4), or because AF was triggered during the procedure (#5,8).

Myocardial sleeve length

Overall, the length of the myocardial sleeve was 36 $\pm$ 17 mm. Although there was marked variability between the PVs, the inferior veins have shorter muscle sleeves (30 $\pm$ 11 mm) compared to the superior veins (44 $\pm$ 19 mm, $P = 0.015$) (Table 1). The RSPV was observed to have the longest myocardial sleeve and the largest diameter (Table 1). The distance from the start of the PV ostia to the most distal electrical point within each ostium was measured and represents the length of the myocardial sleeve.

Electrophysiological characteristics of the pulmonary veins

Overall, the voltage within the PVs was 1.2 $\pm$ 1.4 mV, whereas the voltage of the adjacent LA posterior wall was significantly higher (3.4 $\pm$ 0.9 mV, $P < 0.001$). The superior veins had significantly higher voltages (1.8 $\pm$ 1.8 mV) than the inferior veins (0.7 $\pm$ 0.8 mV, $P = 0.013$). The earliest left atrial activation was observed in the RSPV closest to Bachmann's bundle (Fig. 2). The morphology of the PV electrograms showed a fast upstroke and short duration (Fig. 3). The percentage of area with electrically normal functioning tissue within each vein was above 54 $\pm$ 31 % (Table 1). The conduction velocity was significantly higher in the LIPV (230 $\pm$ 40 cm/s)

Table 1 Overview of data from the voltage maps collected from nine horses in sinus rhythm.

	LIPV	RIPV	LSPV	RSPV
Number of ostia identified	8	9	8	9
Used points	89 ± 56	139 ± 65	99 ± 104	193 ± 113
Myocardial sleeve length (mm)	31 ± 11	28 ± 13	38 ± 13[a]	49 ± 22[a]
Mean ostium diameter (mm)	31 ± 8	42 ± 7	35 ± 5	51 ± 18
Peak-to-peak voltage (mV)	0.8 ± 1.0	0.6 ± 0.5	2.5 ± 2.5[b]	1.2 ± 0.5[b]
Conduction velocity (cm/s)	230 ± 40[c]	170 ± 40	220 ± 51	170 ± 30
Area (%) between 0.05 and 0.5 mV	42 ± 35	24 ± 18	18 ± 21	26 ± 27
Area (%) above 0.5 mV	73 ± 45	54 ± 31	82 ± 32	81 ± 31

Abbreviations: LIPV: left inferior pulmonary vein; LSPV: left superior pulmonary vein; RIPV: right inferior pulmonary vein; RSPV: right superior pulmonary vein.
Data presented as mean ± standard deviation. Myocardial sleeve length (mm) was measured from the ostia opening to the most distal electrical point of each PV. Peak-to-peak voltage in millivolts (mV). Conduction velocity in cm/s. Area (%) is the percentage of area mapped to the most distal electrical point within each vein between and above voltage thresholds.
[a] Superior veins were significantly longer than inferior veins (P = 0.015).
[b] Superior veins had a significantly higher voltage that inferior veins (P = 0.013).
[c] Conduction velocity in the LIPV was significantly higher than the RIPV (P = 0.037) and RSPV (P = 0.013).

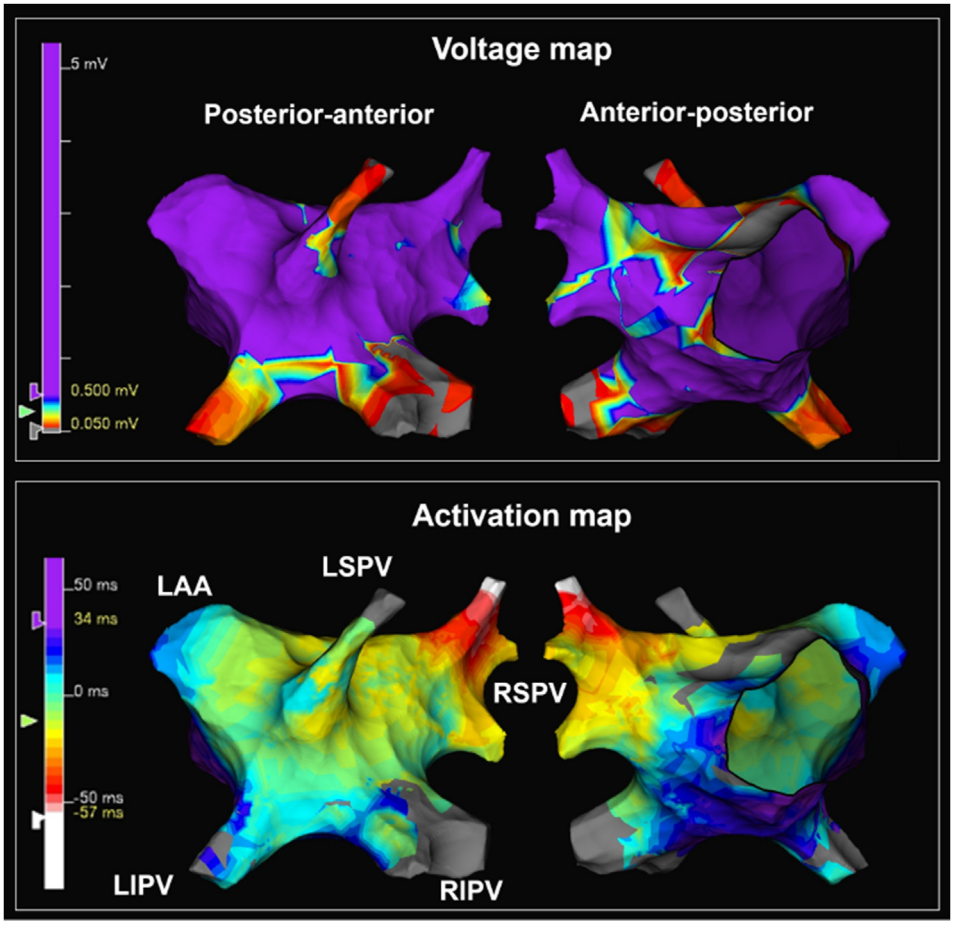

Figure 2 Electro-anatomical maps. Three-dimensional electro-anatomical maps of left atrium (LA) including the pulmonary veins (PV) in anterior-posterior and posterior-anterior view of LA map from EnSite Precision. First row: Voltage map shows peak-to-peak voltage in millivolts (mV). Second row: Local activation time map with the earliest activated tissue being white/red and the latest being dark blue. Grey areas are areas with either poor contact or no electrical signals as seen in the distal part of the PV. LAA: left atria appendage; LIPV: left inferior pulmonary vein; LSPV: left superior pulmonary vein; RIPV: right inferior pulmonary vein; RSPV: right superior pulmonary vein.

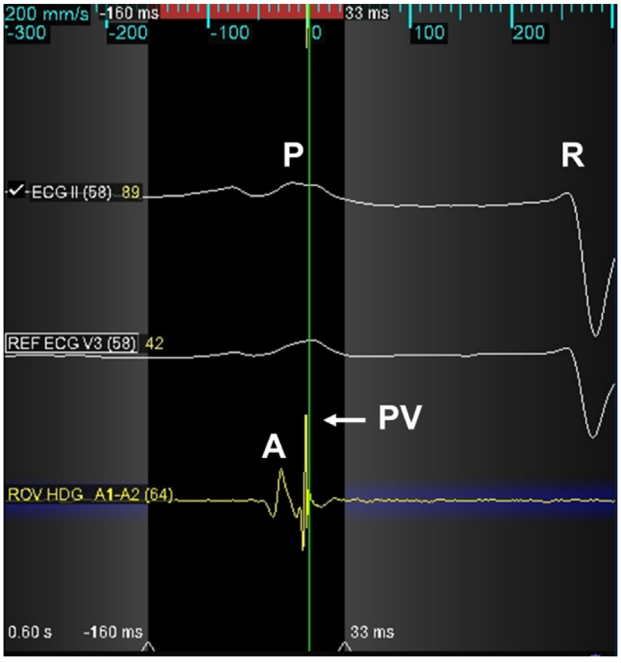

Figure 3 Depolarization of pulmonary vein myocardium. Pulmonary vein (PV) signal recorded with a high-density (HD) grid using EnSite Precision. First two traces show surface electrocardiogram with P-wave (P) and R-wave (R), where peak-P served as time reference (lead II and V3, paper speed 200 mm/s). The deflection of the PV depolarization (white arrow) recorded with the HD grid was preceded by a far-field left atrial activation (A). Far-field signals are recognized as having blunted amplitude and a decreased slope. Black vertical area shows the roving activation window.

compared to RSPV (170 ± 30 cm/s, P = 0.013), RIPV (170 ± 40 cm/s, P = 0.037) and the LA posterior wall (165 ± 14 cm/s, P < 0.001) (Table 1). Results from each horse are presented in supplemental Table C and Table D (available online).

Areas at the veno-atrial junction with reduced conduction

The veno-atrial junction demonstrated significant areas of slow conduction. This was apparent during sinus rhythm mapping in three horses and were characterized as areas of isochronal crowding observed on the activation maps, where areas with reduced conduction could be recognized as a reduced distance between the isochronal lines (Fig. 4). The areas with isochronal crowding were located at the veno-atrial junction in the RSPV and RIPV.

Structural characteristics of the pulmonary vein myocardium

From the histological analysis, it was visible that there was a considerable variation in myocardial fibre orientation in the veno-atrial junction, whereas the fibres were more organized in a longitudinal direction distally (Fig. 5A). The percentage of fibrosis was significantly higher in PV (26.1 ± 6.6 %), compared to both RA (17.2 ± 4.9 %, P = 0.005) and LA (14.5 ± 5.1 %, P = 0.003), whereas there was no significant difference between LA and RA (Fig. 5B).

The expression of $Ca_V1.2$ was significantly higher in PV than LA (P = 0.001) (Fig. 6) and supplemental Table E (available online). Both RyR2 (P = 0.032) and small conductance calcium-activated potassium channel 3 (P = 0.032) were significantly higher in LA than RA, but there were no differences between LA and PV. Expression of $Ca_V3.3$ and connexin-43 were equal at all three sites (Fig. 6) and supplemental Table E (available online). Immunohistochemical staining for HCN4 was negative.

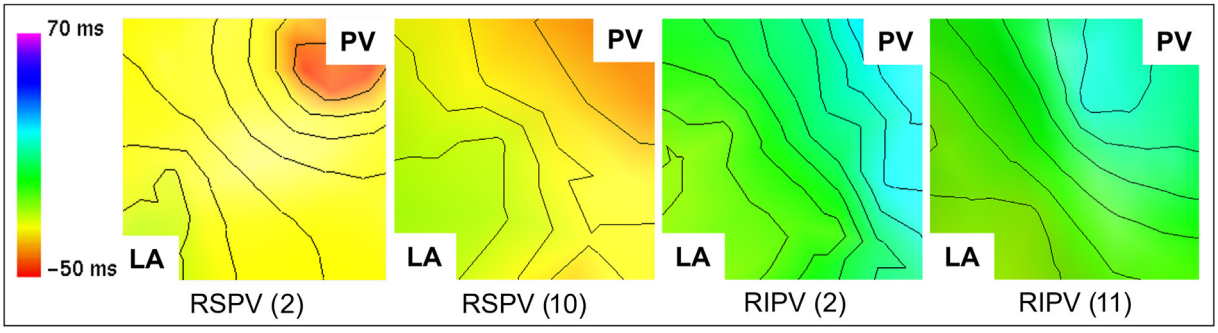

Figure 4 Isochronal activation maps. Activation maps from the veno-atrial junction with isochronal lines showing the velocity of the propagation wave with 5 ms between each line. Areas with fast conduction have a longer distance between the lines whereas areas with reduced conduction are areas where the distance between the isochrones become smaller. Colour scale indicates time of activation from the time reference point (peak of P-wave). From left: right superior PV (RSPV) (2), RSPV (10), right inferior PV (RIPV) (2), RIPV (11).

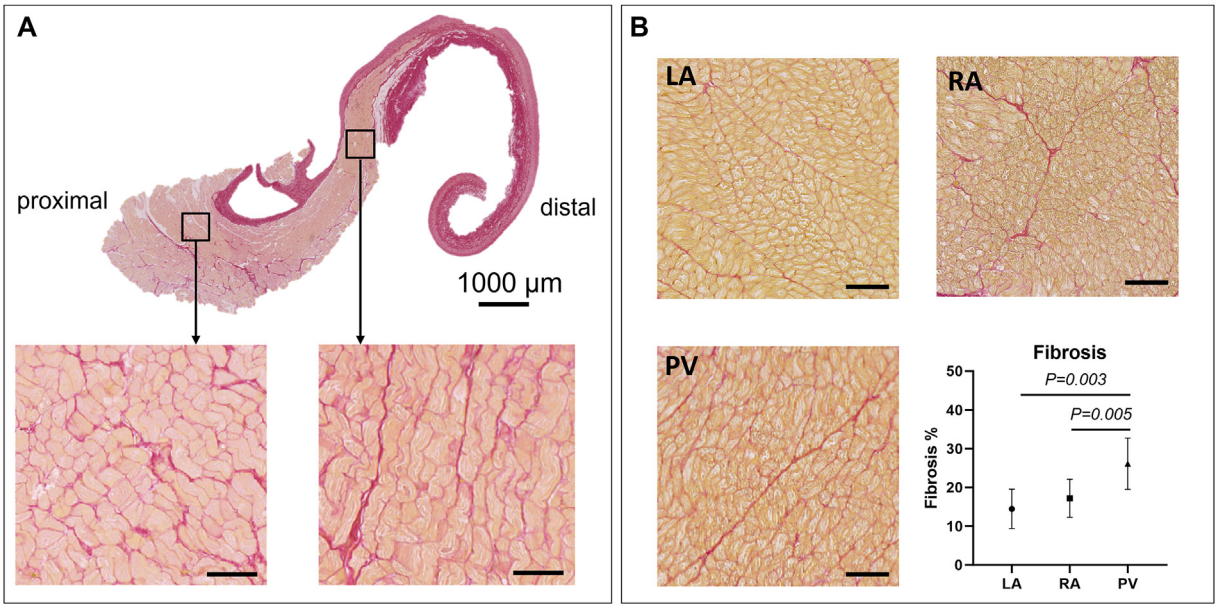

Figure 5 Histological imaging with Picro-sirius red. Tissue stained with Picro-sirius red shows fibrosis as red (scale bar 50 µm when nothing else is annotated). A) The proximal part of the pulmonary vein, located near the atria, exhibits a complex fibre orientation, while the myocardial sleeve, extending towards the lung shows linear fibre orientation. B) Tissue samples used to compare the percentage of fibrosis surrounding the myocardium in three different sites. Pulmonary vein samples appear more red as they have a higher percentage of fibrosis. Graph presents mean percentage of fibrosis and standard deviation. LA: left atrium; RA: right atrium; PV: pulmonary vein.

Discussion

This study characterizes the structural and electro-anatomical features of the equine pulmonary veins. Other than demonstrating the feasibility of 3D electro-anatomical mapping of PVs in standing sedated horses using a retrograde approach, it provides several new information: First, the equine subject has electrically active myocardial sleeves within the PVs, which are longer in the superior compared to the inferior PVs. Second, the PVs demonstrate unique electrophysiological and histological properties compared to the adjacent atria. In particular, there was heterogeneity in myocardial fibrosis, ion channel distribution, voltage and conduction at the veno-atrial junction and the PVs compared to the atria. These unique features demonstrate that horses have the necessary structural, electrical, and ionic milieu that implicates this region in initiation and maintenance of arrhythmia.

The geometry of four PV ostia was identified in most horses; however, variation in the number of veins can occur [17]. We found the RSPV easiest to access, and it was the largest ostia with up to three branching veins with long myocardial sleeves, as described in macro-anatomical studies [17]. The superior veins had longer myocardial sleeves, similar to humans [8,26]. In humans, the larger superior veins also represent the area where most AF triggering ectopy originates from [8]. Histologically, we found a significantly higher percentage of fibrosis in the PV compared to LA and RA, similar to those previously reported by Saljic et al. [18] using comparable methods. We observed a large variation in the orientation of the cardiomyocytes within the veno-atrial junction, similar to previous findings in horses, sheep, dogs, and humans [11,13,16,27,28]. An increase in extracellular matrix and a heterogenic myocardium can reduce conduction velocity, which may cause conduction block, facilitate micro re-entry, and promote AF [10,29—31].

The voltage at the veno-atrial junction was lower than the LA posterior wall, further decreasing distally into the veins (Fig. 2). The earliest activation was observed closest to the RSPV, which is closest to the atrial septum and Bachmann's bundle, similar to what has previously been described in horses [32,33] (Fig. 2).

The conduction velocity of the PVs was higher than previously reported in atrial tissue in horses, but similar to previously reported velocities in fast conduction areas such as the dorsal RA [32]. Both RSPV and RIPV had significantly slower conduction velocities than the LIPV. Similarly, areas of reduced conduction were observed on isochronal maps at the veno-atrial junction of RSPV and RIPV.

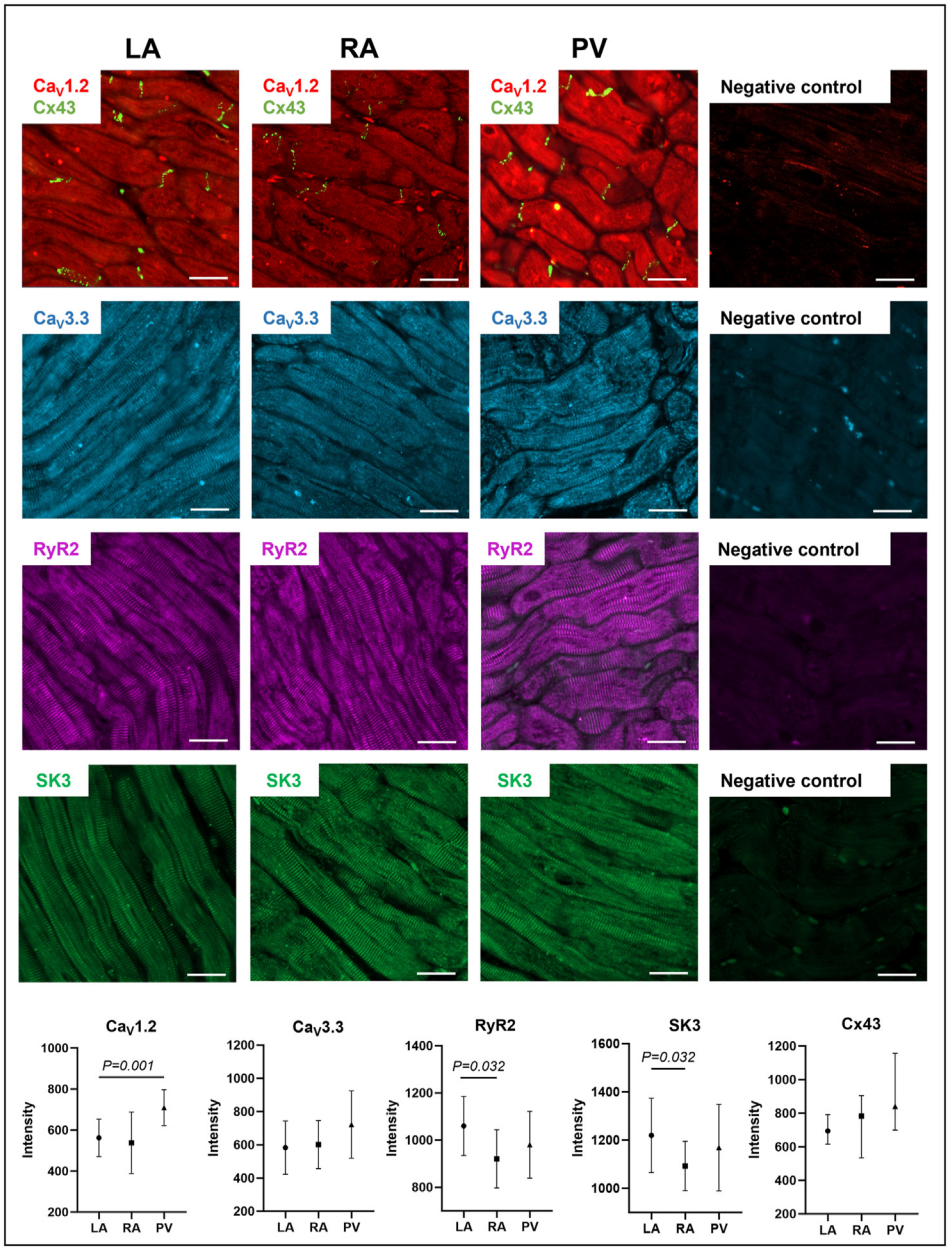

Figure 6 Immunohistochemical imaging analyses. Immunohistochemistry of the myocardium in the left atrium (LA), right atrium (RA) and pulmonary veins (PV) including negative controls (scale bar 20 μm). From top; $Ca_V1.2$: L-type calcium channels (red); Cx43: connexin-43 (green); $Ca_V3.3$: T-type calcium channels (blue); RyR2: ryanodine receptor-2 (purple); SK3: small conductance calcium-activated potassium channel 3 (dark green). The graphs below show results from the ion channel expression analyses quantifying the fluorescence intensity of $Ca_V1.2$, $Ca_V3.3$, RyR2, SK3, and Cx43. Y-axis shows the amount of intensity, defined as the number of grey tones expressed. Data presented as mean and standard deviation.

However, we were not able to compare it with the histology from the specific sites.

In humans, the RSPV is the main site for conduction block [8], most likely because of the density and myocardial heterogeneity. This has also been described in animal studies in dogs and sheep, where reduced conduction was found in areas of variable myocyte orientation [13,27,34]. Ideally, pacing within each vein from a proximal and distal aspect could lead to more accurate measurements. The precision of these measurements could have been affected by inaccuracies in geometric scaling, as conduction velocity measurements rely on spatial resolution. Further studies investigating the endocardial conduction velocity in horses are needed.

The expressed proteins $Ca_V1.2$, $Ca_V3.3$ and RyR2 play a role in calcium flux and handling. Altered calcium handling function can cause triggered activity such as early after-depolarizations and delayed after-depolarizations. Early after-depolarizations occurs when the calcium channels are reactivated in early phase 2 of the depolarization, and delayed after-depolarizations is initiated by an additional calcium release from the sarcoplasmic reticulum late in the repolarization phase [29,35]. The $Ca_V3.3$ is a fast voltage-gated calcium channel (T-type) and together with $Ca_V1.2$, a slow voltage-gated calcium channel (L-type), are activated in the early phase 2 of the action potential and mediates calcium influx to the cell. We located both proteins in the t-tubules of atrial and PV myocytes.

Previous studies in canines compared the expression of $Ca_V1.2$ in PV and LA using Western blot but did not find a different expression in the atrial and PV tissue [20]. Studies investigating the I_{Ca}-current found it smaller in the PV myocytes [21]. However, a higher cellular density of $Ca_V1.2$ is not directly correlated to the function, as this depends on the phosphorylation processes, regulating the ion channel activation. Nevertheless, a higher density of $Ca_V1.2$ could enhance the risk of early after-depolarizations and arrhythmias [35]. We identified a higher expression of $Ca_V1.2$ in PVs than in LA, which could explain why early after-depolarizations may occur more frequently from PV myocytes.

None of the investigated tissue expressed HCN4, the primary channel responsible for the I_f-current, which is highly involved in the pacemaker activity in nodal tissue [36]. The presence of HCN4 has been hypothesized to be a reasonable explanation for any spontaneous electrical activity in the heart, including the PVs, which has led others to explore the expression of HCN4 in various cardiac sites as well [19,37]. In rats, HCN4 was found to be expressed in nodal tissue but not PV [19], whereas a recent study in dogs showed that HCN4 was indeed detected in atrial and PV samples using polymerase chain reaction analysis and western blotting [37]. However, they did find the expression of HCN4 to be higher in nodal tissue compared to other sites. Identifying antibodies specific to equine proteins can pose a considerable challenge. While the staining of HCN4 in our study yielded negative results, it is important to note that the same antibody had previously demonstrated successful application in equine nodal tissue [38]. Nevertheless, it is essential to acknowledge that our investigation focussed on smaller regions, and we cannot definitively exclude the possibility of HCN4 presence elsewhere within the atria. Further investigations in horses are needed to clarify if HCN4 is present in PVs.

The RyR2 was equally expressed in the atria and PV. Ryanodine receptor-2 is responsible for the calcium-induced calcium release function of the sarcoplasmic reticulum within the cardiomyocyte [39]. Dysregulation of RyR2, meaning disturbances of intracellular calcium, may result in delayed after-depolarizations and it has been shown that this receptor is increased in people with paroxysmal AF [9]. It has been shown that RyR2 is hyperphosphorylated with increased sympathetic activity, and a blockade of the sympathetic system resulted in reduced spontaneous PV automaticity [29]. It could be hypothesized that AF in horses occurring during racing could originate from increased sympathetic hyperphosphorylation of the RyR2.

Despite this study's characterization of some ionic components of equine PV myocytes, the molecular functions and regulatory mechanisms are yet to be investigated. Furthermore, the role of the autonomic nervous system in relation to AF pathophysiology is not fully understood [10,40,41], but may be relevant in cases of spontaneous PV activity. Like humans, horses undergo frequent changes in the autonomic tone, which may trigger AF [5]. Moreover, the PVs are closely located to neurons and ganglia, which may interplay with PV ectopy [16].

We used a retrograde approach to access LA through the carotid artery passing the aortic and mitral valves. This approach requires a cut down to the carotid artery, which in patients would require suturing or placement of an occlusion device after the procedure. With this method, the path to reach the PV is long and may explain why we could not identify all ostia and bifurcations. In humans, a transseptal approach through the foramen ovale is used to access LA, and this approach is currently being validated in horses.[x] The PVs were previously identified using a different electro-anatomical mapping system with the horses in general anaesthesia [32,42]. Both methods have been shown to be feasible and as more studies are being performed, we may be able to scrutinize the role of spontaneous PV activity in AF pathogenesis in horses.

[x] Vernemmen I, Van Steenkiste G, E. B, Schauvliege S, Cornelis K, Decloedt A et al. Transseptal puncture guided by intracardiac ultrasound to access the left atrium in adult horses. 15th. ECEIM Congr. Online Proc. B., Rome: ECEIM; 2022, p. 113.

Several limitations need to be considered in this study. This study included only a small number of horses. Mapping undertaken as described was developed during the study and necessarily required evaluation in a small group of animals. The definition of low-voltage signals was based on a previous study investigating RA in horses [25] and the definitions used in human medicine, however, this may not be adaptable to the left atrium. We used an impedance-based mapping system that is clinically used in humans; whether there are inaccuracies in the translation of use in the current study in much larger and vertically positioned subjects has not been validated. In addition, mapping was only performed in sinus rhythm, which is likely to underestimate the degrees of heterogeneity of the myocardium. We did not undertake mapping during pacing at different sites and rates that would further exemplify the conduction abnormalities. We used xylazine, known to exhibit negative chronotropic effects. However, we do believe that a standing procedure simulates the true physiological conditions more than when the horses undergo general anaesthesia. Finally, only some tissue samples included the most distal part of the PV, therefore the histological and immunohistochemical analysis could not be divided into a proximal and distal region. Ideally, sections from all PVs should have been harvested from each horse to confirm the number of veins and myocardial sleeve length. Future studies investigating the equine PVs should consider including a pacing protocol to measure conduction velocity and refractoriness within different areas of the PVs. In this study, we did not observe any complex fractionated electrograms. Regardless, investigation of fractionated electrograms and a specific definition of these is needed in horses.

Conclusion

This study identified structural and electro-anatomical differences between the PV and LA myocardium in healthy horses. Structurally the PV myocardium expressed more L-type calcium channels and a higher amount of fibrosis than the LA myocardium. Using 3D electro-anatomical mapping, the veno-atrial junction had lower voltages compared to the adjacent atria. The superior veins differed from the inferior veins by having longer sleeves and higher voltages. The heterogeneous myocardial sleeves with complex myocardial fibre orientation and areas of decreased conduction in the veno-atrial junction provide a milieu for re-entry and AF initiation. Further investigations of the remodelled PVs and knowledge of PV isolation procedures are essential for future understanding and treatment of AF in horses.

Funding

Dr Sanders is supported by the National Health and Medical Research Council of Australia.

Conflicts of Interest Statement

Mr Kutieleh is an employee of Abbott Medical, Australia. Dr Sanders reports having served on the advisory board of Boston Scientific, CathRx, Medtronic, Abbott Medical and Pacemate. Dr Sanders reports that the University of Adelaide has received on his behalf lecture and/or consulting fees from Medtronic, Boston-Scientific, and Abbott Medical, Pacemate and CathRx. Dr Sanders reports that the University of Adelaide has received on his behalf research funding from Medtronic, Abbott Medical, Boston-Scientific, Pacemate, Becton Dickinson and Microport. The remaining authors do not have any conflicts of interest to disclose.

Acknowledgements

We would like to thank Susanne Nørskov Sørensen for her technical assistance in the laboratory. We would like to express our sincere gratitude to Pawel Kuklik for his invaluable technical assistance and facilitation of software for data analysis.

Supplementary data

Supplementary data associated with this article can be found, in the online version, at https://doi.org/10.1016/j.jvc.2024.01.001.

References

[1] Reef VB, Bonagura J, Buhl R, Mcgurrin MKJ, Schwarzwald CC, van Loon G, Young LE. Recommendations for management of equine athletes with cardiovascular abnormalities. J Vet Intern Med 2014;28:749—61.
[2] Decloedt A, Van Steenkiste G, Vera L, Buhl R, van Loon G. Atrial fibrillation in horses Part 2: diagnosis, treatment and prognosis. Vet J 2021;268:105594.
[3] Kjeldsen ST, Nissen SD, Buhl R, Hopster-Iversen C. Paroxysmal atrial fibrillation in horses: pathophysiology, diagnostics and clinical aspects. Animals 2022;12:698.

[4] Kjeldsen ST, Jensen M, Sørensen CT, Hopster-Iversen C, Nissen SD. Long-term monitoring with an implantable loop recorder detects multiple episodes of paroxysmal atrial fibrillation after electrical cardioversion in a Warmblood horse. Equine Vet Educ 2022:1—7.
[5] Decloedt A, Van Steenkiste G, Vera L, Buhl R, van Loon G. Atrial fibrillation in horses part 1: pathophysiology. Vet J 2020;263:105521.
[6] Haïssaguerre M, Jaïs P, Shah DC, Takahashi A, Hocini M, Quiniou G, Garrigue S, Le Mouroux A, Le Métayer P, Clémenty J. Spontaneous initiation of atrial fibrillation by ectopic beats originating in the pulmonary veins. N Engl J Med 1998;339:659—66.
[7] Lau DH, Linz D, Schotten U, Mahajan R, Sanders P, Kalman JM. Pathophysiology of paroxysmal and persistent atrial fibrillation: rotors, foci and fibrosis. Heart Lung Circ 2017;26:887—93.
[8] Chen S-A, Hsieh M-H, Tai C-T, Tsai C-F, Prakash VS, Yu W-C, Hsu T-L, Ding Y-A, Chang M-S. Initiation of atrial fibrillation by ectopic beats originating from the pulmonary veins. Circulation 1999;100:1879—86.
[9] Voigt N, Heijman J, Wang Q, Chiang DY, Li N, Karck M, Wehrens XHT, Nattel S, Dobrev D. Cellular and molecular mechanisms of atrial arrhythmogenesis in patients with paroxysmal atrial fibrillation. Circulation 2014;129:145—56.
[10] Nattel S, Dobrev D. Electrophysiological and molecular mechanisms of paroxysmal atrial fibrillation. Nat Rev Cardiol 2016;13:575—90.
[11] Moubarak JB, Rozwadowski JV, Strzalka CT, Buck WR, Tan WS, Kish GF, Kisiel T, Fronc HC, Maloney JD. Pulmonary veins-left atrial junction: anatomic and histological study. Pacing Clin Electrophysiol 2000;23:1836—8.
[12] Haïssaguerre M, Sanders P, Hocini M, Jaïs P, Clémenty J. Pulmonary veins in the substrate for atrial fibrillation: the "venous wave" hypothesis. J Am Coll Cardiol 2004;43:2290—2.
[13] Hocini M, Ho SY, Kawara T, Linnenbank AC, Potse M, Shah D, Jaïs P, Janse MJ, Haïssaguerre M, Se Bakker JMT. Electrical conduction in canine pulmonary veins: electrophysiological and anatomic correlation. Circulation 2002;105:2442—8.
[14] Hamabe A, Okuyama Y, Miyauchi Y, Zhou S, Pak HN, Karagueuzian HS, Fishbein MC, Chen PS. Correlation between anatomy and electrical activation in canine pulmonary veins. Circulation 2003;107:1550—5.
[15] Linz D, Hesselkilde E, Kutieleh R, Jespersen T, Buhl R, Sanders P. Pulmonary vein firing initiating atrial fibrillation in the horse: oversized dimensions but similar mechanisms. J Cardiovasc Electrophysiol 2020;31:1211—2.
[16] Vandecasteele T, Van Den Broeck W, Tay H, Couck L, van Loon G, Cornillie P. 3D reconstruction of the porcine and equine pulmonary veins, supplemented with the identification of telocytes in the horse. Anat Histol Embryol 2018;47:145—52.
[17] Vandecasteele T, van Loon G, Vandevelde K, De Pauw B, Simoens P, Cornillie P. Topography and ultrasonographic identification of the equine pulmonary vein draining pattern. Vet J 2016;210:17—23.
[18] Saljic A, Friederike Fenner M, Winters J, Flethøj M, Eggert Eggertsen C, Carstensen H, Dalgas Nissen S, Melis Hesselkilde E, van Hunnik A, Schotten U, Sørensen U, Jespersen T, Verheule S, Buhl R. Increased fibroblast accumulation in the equine heart following persistent atrial fibrillation. IJC Hear Vasc 2021;35:100842.
[19] Xiao Y, Cai X, Atkinson A, Logantha SJ, Boyett M, Dobrzynski H. Expression of connexin 43, ion channels and Ca2+-handling proteins in rat pulmonary vein cardiomyocytes. Exp Ther Med 2016;12:3233—41.
[20] Melnyk P, Ehrlich JR, Pourrier M, Villeneuve L, Cha TJ, Nattel S. Comparison of ion channel distribution and expression in cardiomyocytes of canine pulmonary veins versus left atrium. Cardiovasc Res 2005;65:104—16.
[21] Ehrlich JR, Cha TJ, Zhang L, Chartier D, Melnyk P, Hohnloser SH, Nattel S. Cellular electrophysiology of canine pulmonary vein cardiomyocytes: action potential and ionic current properties. J Physiol 2003;551:801—13.
[22] Hesselkilde EZ, Carstensen H, Flethøj M, Fenner M, Kruse DD, Sattler SM, Tfelt-Hansen J, Pehrson S, Braunstein TH, Carlson J, Platonov PG, Jespersen T, Buhl R. Longitudinal study of electrical, functional and structural remodelling in an equine model of atrial fibrillation. BMC Cardiovasc Disord 2019;19:228.
[23] Haugaard MM, Hesselkilde EZ, Pehrson S, Carstensen H, Flethøj M, Præstegaard KF, Sørensen US, Diness JG, Grunnet M, Buhl R, Jespersen T. Pharmacologic inhibition of small-conductance calcium-activated potassium (SK) channels by NS8593 reveals atrial antiarrhythmic potential in horses. Heart Rhythm 2015;12:825—35.
[24] Finley MR, Li Y, Hua F, Lillich J, Mitchell KE, Ganta S, Gilmour RF, Freeman LC. Expression and coassociation of ERG1, KCNQ1, and KCNE1 potassium channel proteins in horse heart. Am J Physiol Heart Circ Physiol 2002;283:126—38.
[25] Hesselkilde E, Linz D, Saljic A, Carstensen H, Kutieleh R, Jespersen T, Sanders P, Buhl R. First catheter-based high-density endocardial 3D electroanatomical mapping of the right atrium in standing horses. Equine Vet J 2021;53:186—93.
[26] Nathan N, Eliakim M. The junction between the left atriuni and the pulmonary veins - an anatomic study of human hearts. Circulation 1966;(XXXIV):412—22.
[27] Gottlieb LA, Belterman C, van Amersfoorth S, Loyer V, Constantin M, Hocini M, Dekker LRC, Coronel R. Profibrillatory structural and functional properties of the atrial-pulmonary junction in the absence of remodeling. Front Physiol 2021;12:1—10.
[28] Verheule S, Wilson EE, Arora R, Engle SK, Scott LR, Olgin JE. Tissue structure and connexin expression of canine pulmonary veins. Cardiovasc Res 2002;55:727—38.
[29] Schotten U, Verheule S, Kirchhof P, Goette A. Pathophysiological mechanisms of atrial fibrillation: a translational appraisal. Physiol Rev 2011;91:265—325.
[30] Arora R, Verheule S, Scott L, Navarrete A, Katari V, Wilson E, Vaz D, Olgin JE. Arrhythmogenic substrate of the pulmonary veins assessed by high-resolution optical mapping. Circulation 2003;107:1816—21.
[31] Jaïs P, Hocini M, Macle L, Choi KJ, Deisenhofer I, Weerasooriya R, Shah DC, Garrigue S, Raybaud F, Scavee C, Le Metayer P, Clémenty J, Haïssaguerre M. Distinctive electrophysiological properties of pulmonary veins in patients with atrial fibrillation. Circulation 2002;106:2479—85.
[32] Van Steenkiste G, Vera L, Decloedt A, Schauvliege S, Boussy T, van Loon G. Endocardial electro-anatomic mapping in healthy horses: normal sinus impulse propagation in the left and right atrium and the ventricles. Vet J 2020;258:105452.
[33] Hamlin R, Smetzer D, Senta T, Smith C. Atrial activation paths and P waves in horses. Am J Physiol Content 1970;219:306—13.
[34] Okuyama Y, Miyauchi Y, Park AM, Hamabe A, Zhou S, Hayashi H, Miyauchi M, Omichi C, Pak HN, Brodsky LA, Mandel WJ, Fishbein MC, Karagueuzian HS, Chen PS. High resolution mapping of the pulmonary vein and the vein of

marshall during induced atrial fibrillation and atrial tachycardia in a canine model of pacing-induced congestive heart failure. J Am Coll Cardiol 2003;42:348—60.
[35] Schmitt N, Grunnet M, Olesen SP. Cardiac potassium channel subtypes: new roles in repolarization and arrhythmia. Physiol Rev 2014;94:609—53.
[36] Yamamoto M, Dobrzynski H, Tellez J, Niwa R, Billeter R, Honjo H, Kodama I, Boyett MR. Extended atrial conduction system characterised by the expression of the HCN4 channel and connexin45. Cardiovasc Res 2006;72:271—81.
[37] Li YD, Hong YF, Zhang Y, Zhou XH, Ji YT, Li HL, Xu GJ, Li JX, Sun L, Zhang JH, Xin Q, Yusufuaji Y, Xiong J, Tang BP. Association between reversal in the expression of hyperpolarization-activated cyclic nucleotide-gated (HCN) channel and age-related atrial fibrillation. Med Sci Mon Int Med J Exp Clin Res 2014;20:2292—7.
[38] Mesirca P, Nakao S, Nissen SD, Forte G, Anderson C, Trussell T, Li J, Cox C, Logantha S, Sana Yaar, Carstensen H, Bidaud I, Stuart Soattin L, Morris GM, da Costa Martinas PA, Cartwright EJ, Oceandy D, Mangoni ME, Jespersen T, Buhl R, Dobrzynski H, Boyett MR, D'Souza A. Intrinsic electrical remodeling underlies atrioventricular block in athletes. Circ Res 2021;129:E1—20.
[39] Dobrev D, Voigt N, Wehrens XHT. The ryanodine receptor channel as a molecular motif in atrial fibrillation: pathophysiological and therapeutic implications. Cardiovasc Res 2011;89:734—43.
[40] Linz D, Elliott AD, Hohl M, Malik V, Schotten U, Dobrev D, Nattel S, Böhm M, Floras J, Lau DH, Sanders P. Role of autonomic nervous system in atrial fibrillation. Int J Cardiol 2019;287:181—8.
[41] Chen PS, Chen LS, Fishbein MC, Lin SF, Nattel S. Role of the autonomic nervous system in atrial fibrillation: pathophysiology and therapy. Circ Res 2014;114:1500—15.
[42] Van Steenkiste G, De Clercq D, Boussy T, Vera L, Schauvliege S, Decloedt A, van Loon G. Three dimensional ultra-high-density electro-anatomical cardiac mapping in horses: methodology. Equine Vet J 2020;52:765—72.